Ultrabroadband Spread Spectrum Techniques for Secure Dynamic Spectrum Sharing Above 100 GHz Between Active and Passive Users

Christopher Bosso*, Priyangshu Sen[†], Xavier Cantos-Roman[†], Claire Parisi[†], Ngwe Thawdar[‡] and Josep Miquel Jornet[†]

* Department of Electrical Engineering, University at Buffalo, The State University of New York, NY, USA

† Department of Electrical and Computer Engineering, Northeastern University, Boston, MA, USA

† U.S. Air Force Research Laboratory, Rome, NY, USA

Abstract-In today's technologically driven world, wireless communication has become ubiquitous, and the demand for faster data rates and the ability to support the ever-growing number of devices is higher than ever. The conventional spectrum is overcrowded, motivating research in utilizing higher frequency bands. As new developments in device and physical layer technologies become more accessible, frequencies above 100 GHz show promise to relieve spectrum congestion and enable new high-bandwidth applications that cannot be supported within the current spectrum. Despite the lack of traditional communication systems at these frequencies until very recently, the spectrum above 100 GHz has already been utilized for passive sensing applications, namely, in Earth-exploration satellite services (EESS) with highly sensitive detectors. In order to coexist with these passive users of the spectrum without harmful interference, spread spectrum techniques are proposed as a method to exploit the large available bandwidth at these frequencies while maintaining high data rates and adding an element of security. In this paper, a direct sequence spread spectrum (DSSS) communication system for THz band frequencies is designed, numerically studied and experimentally tested. Successful generation, transmission, and reception of DSSS signals at 130 GHz coexisting with a narrowband interference is demonstrated. Finally, as a study case, the requirements of a DSSS on-the-ground THz backhaul system are derived to ensure coexistence with THz EESS systems.

I. INTRODUCTION

As the number of connected wireless devices continues to steadily rise, the demand for faster data rates substantially increases. Overcrowding in the conventional electromagnetic spectrum in addition to higher bandwidth requirements and the continual rise in connected devices necessitates the use of new spectral bands. Emerging device technologies are now making wireless communication above 100 GHz far more accessible. Numerous applications have been proposed to exploit the unprecedented bandwidth provided by these higher frequency bands [1], [2]. Many of these applications are aimed at achieving very high speed links approaching terabit-persecond data rates. Other applications aim to utilize the large bandwidth available to support many devices all sharing the same frequency bands. It is within this second approach that it is important to address the issue of how we can securely share the medium with other users while minimizing interference.

Despite the term "no man's land" is many times used to refer to the spectrum above 100 GHz, the reality is that there are multiple scientific users of these frequencies. These include,

for example, NASA's Aura satellite and its Microwave Limb Sounder (MLS), which collects radiometric data at 118 GHz, 190 GHz, 240 GHz, 640 GHz, and 2.5 THz [3]. Remote sensing and Earth Exploration satellites services (EESS), like Aura, have very highly sensitive detectors for Earth-observation purposes with maximum interference thresholds on the order of -166 dBW [4]. Therefore, it is crucial that any actively transmitting users in the spectrum above 100 GHz take measures to minimize all possible interference with passive users. For the time being, the solution has relied on prohibiting the active use of specific bands dedicated to scientific passive users of the spectrum, as per the International Telecommunication Union Radiocommunication Sector (ITU-R) Recommendation (Rec.) 5.340. However, the fact that such users are generally satellite-based, the very high propagation losses at frequencies above 100 GHz and the need for very high directional antennas motivates the use of more flexible spectrum sharing techniques between active and passive users [5].

Furthermore, despite the widespread assumption that communications above 100 GHz are more secure due to the high directionality of the transmitted signals and the role of molecular absorption [6], it has been shown that this is not the case [7]. Indeed, the same physics that enable the development of very compact directional antennas at upper millimeter-wave and terahertz (THz) frequencies, also allow very small metallic obstacles to effectively diffract a copy of the transmitted signal between two highly directional users towards directions outside the main transmitter-receiver beam, enabling a smart eavesdropper to recover the original signal. While this phenomenon is true at any frequencies and its impact is less meaningful as we move up in the spectrum (i.e., towards smaller wavelengths), it cannot be ignored [8].

In this paper, we propose the use of DSSS techniques to address both security and coexistence of active and passive users sharing the spectrum above 100 GHz. A DSSS signal is deliberately spread using a unique spreading sequence or code, increasing the overall bandwidth of the transmission. Consequently, DSSS has the advantages of lower susceptibility to jamming, unwanted detection, and the potential for multiple access at the cost of increased bandwidth requirements. Traditionally, DSSS techniques have only been used at slower data rates in applications such as Global Positioning System (GPS) and code-division multiple access (CDMA)

communications, due to its low spectral efficiency compared to techniques such as orthogonal frequency division multiplexing and multiple access (OFDM/OFDMA). However, the very large bandwidth available above 100 GHz relaxes the spectral efficiency requirement and justifies revisiting DSSS for higher speed secure communications and greater coexistence between users. Moreover, DSSS can potentially be implemented at the antenna level [9] and, therefore, without introducing additional requirements on the digital signal processing engine of the system. Thus, there is significant motivation to investigate the practicality of utilizing DSSS techniques above 100 GHz.

The remainder of the paper is organized as follows. In Sec. II, we review the fundamentals behind DSSS as well as the benefits and applications for single-user and multiuser situations. In Sec. III, we analytically derive the impact of narrowband (NB) communication systems on a coexisting DSSS system and vice versa. In Sec. IV, we study through extensive numerical simulation the role of different THz DSSS parameters and coexisting systems on the bit error rate (BER). In Sec. V, we experimentally demonstrate the feasibility of THz DSSS systems for the first time, and validate the requirements for coexistence derived in the previous section. Based on these results, and leveraging the ITU-R recommendations for atmospheric propagation of THz signals, we then explore the possibility to share currently EESS sensing-only bands with on the ground THz systems in Sec. VI. Finally in Sec. VII, we conclude the paper. Ultimately, this paper hopes to demonstrate the potential and feasibility of ultra-broadband DSSS above 100 GHz to dynamically share the spectrum.

II. DSSS SYSTEM MODEL

A. Fundamentals

In DSSS, at the transmitter, each information-bearing symbol is modulated by a bit or *chip* sequence known as a spreading code. The number of chips transmitted or received per second is known as the chip rate. Generally, the chip rate is much higher than the message signal's symbol rate. As a result, the bandwidth of the resulting transmitted signal is larger than that of the information signal. At the receiver, the signal is again multiplied by the same spreading code and integrated over the bit interval to recover the original symbol.

The length of the spreading code, which is also known as the spreading factor (SF), determines the ratio between the chip rate and the unspread symbol rate and, therefore, the factor by which the bandwidth of the spread signal increases. In addition to the length of the spreading code and the data rate, it is also important to consider the type of spreading code used. One category of spreading codes that are of particular interest for spread spectrum communications are pseudonoise (PN) codes. A PN code is a seemingly random binary sequence that can be produced in a deterministic manner. For applications aimed at minimizing multi-user interference, PN spreading codes that have low cross-correlation across a set are desirable. One such example of these desirable PN codes are maximum length sequences (m-sequences) which can be

combined together to generate Gold codes commonly used in GPS and CDMA applications [10].

B. Single-User

For the single-user case, the primary benefits of DSSS lie in its ability to reject NB interference (NBI) and reduce the signal's likelihood of interception. Furthermore, to any users without prior knowledge of the spreading code or chip rate, the spreading operation adds an additional layer of data concealment provided that codes are chosen wisely.

C. Multi-User

In the multi-user case, spread spectrum technology can be utilized for CDMA, a channel access method that enables multiple users to share the same frequency band simultaneously. By spreading each user with unique codes that have low cross-correlation properties, users can be separated at the receiver with the despreading process and other users will be completely rejected (in the case of orthogonal codes) or appear as a minimal amount of noise (in the case of PN codes).

III. SPECTRUM SHARING WITH NARROW-BAND USERS

With a focus on coexistence in the above 100 GHz frequency band, DSSS presents several distinct advantages for both passive and active users. For active users, DSSS allows for the rejection of NBI from coexisting NB active users as well as other spread users as long as a unique spreading code with low cross-correlation is used. On the other hand, the spreading of the signal reduces the power at any given frequency allowing the DSSS signal to be hidden in the noise. For passive users like NASA's Aura satellite, this reduction of power can be tuned so that at any given time the power of the signal at the target frequency is reduced below the detection threshold for the instrument.

A. Impact of Narrowband Interference on DSSS Performance

In this section, we review the theory behind DSSS and its advantages for rejection of NBI. The complex baseband modulated signal can be defined as $x(t) = \sum x_n g(t - nT_s)$, where g(t) denotes the pulse, T_s is the symbol duration, and x_n refers to the complex-mapped symbol (I+jQ) transmitted at the nth symbol time. After spreading, the baseband DSSS signal is represented by,

$$x_{\text{DSSS}}(t) = \sum_{n} \sum_{m} x_n s_m g_c(t - mT_c) g(t - nT_s),$$

$$= \sum_{n} x_n s_c(t) g(t - nT_s),$$
 (1)

where m denotes mth chip, T_c is the chip period and g_c is the pulse utilized for chip. Further, $s_c(t)$ denotes the full spreading code and is given by $s_c(t) = \sum s_m g_c(t-mT_c)$. This signal can be upconverted and transmitted by frequency mixing by considering the real part of the modulated signal. However, the performance of DSSS is presented in the complex baseband domain, and it can easily be extended for real analysis considering I and Q components separately.

In this analysis, for simplicity, we assume that there is no multipath component, the receiver is synchronized and the bits are demodulated symbol basis. In the presence of a NBI, Z(t), with channel impulse response, $h(t) = \delta(t)$, and additive white Gaussian noise (AWGN), n(t), the recovered unspread signal at the receiver is represented by,

$$r_n(t) = x_n(t)s_c^2(t) + n(t)s_c(t) + Z(t)s_c(t).$$
 (2)

Because $s_c^2(t) = 1$, the spreading code sequence can be separated from the data signal. At the demodulator, the complex recovered symbol, \hat{x}_n , can be defined as:

$$\hat{x}_{n} = \frac{1}{T_{s}} \int_{0}^{T_{s}} x_{n} dt + \sqrt{\frac{1}{T_{s}}} \int_{0}^{T_{s}} n(t) s_{c}(t) dt + \sqrt{\frac{1}{T_{c}}} \int_{0}^{T_{s}} Z(t) s_{c}(t) dt.$$
(3)

Because $Z(t)s_c(t)$ is now a wideband signal with a bandwidth of approximately $1/T_c$, and the integration acts as a lowpass filter with a bandwidth of $1/T_s$ where $1/T_s \ll 1/T_c$, most of the energy of the interfering symbol is removed [11]. The factor by which the power of the interfering signal is reduced is known as the spreading or processing gain (G_p) and is defined as

$$G_p = \frac{T_s}{T_c}. (4)$$

The processing gain is the ratio of the bandwidth of the spread signal to the bandwidth of the data signal. Therefore, as the processing gain increases, we can achieve greater spreading of the power spectral density (PSD) of the signal and a resulting increase in rejection of NBI.

B. Impact of DSSS signals on Narrowband Passive Users

While DSSS is effective in reducing unwanted NBI to the spread signal, it also has the effect of reducing peak PSD assuming the total energy is preserved. This is because as the signal is spread, the average signal power is distributed over the larger bandwidth leading to lower peak PSD at any given frequency compared to the NB signal as shown in Fig. 1. Further, the envelope (upper) of PSD of the DSSS becomes more uniform with an increase of the SF. This effect has been frequently used in tactical communication systems for low probability of detection (LPD) or low probability of intercept (LPI) applications [12]. However, this same effect can also be beneficial for coexistence between active and passive users. If the PSD of the DSSS signal is reduced below the maximum detector threshold for a satellite,å then there would be no issues in sharing frequencies and transmitting times at frequencies above 100 GHz, as we discuss in Sec. VI. This reduction in peak spectral density is proportional to the processing gain, G_p . Thus, greater spreading over a wider bandwidth results in a greater reduction in peak PSD.

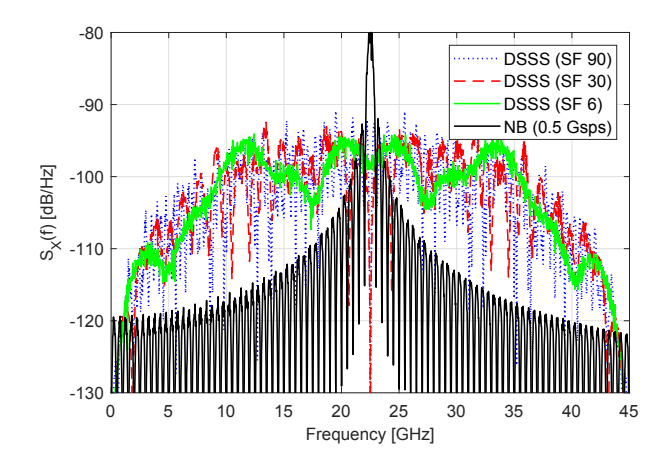


Fig. 1. Power spectral density of the DSSS (4-QAM) with different SF and the NB (4-QAM) signal.

IV. NUMERICAL PERFORMANCE ANALYSIS

In this section, a numerical study is performed to examine the BER performance of broadband DSSS and NB signals in the presence of each other, while both having the same received power. The BER plots are generated in the presence of AWGN. For DSSS, a fixed intermediate frequency (IF) bandwidth of 45 GHz (i.e., signal with the 22.5 Gigachips-persecond (Gcps) chip rate) is considered while using different SF (i.e., various symbol rate). Further, a NB signal with bandwidth up to 4 GHz or symbol rate up to 2 Gigasymbols-persecond (Gsps) modulated at different intermediate frequency (IF) frequencies within the bandwidth limit (i.e., 45 GHz) is considered. Both the DSSS and NB signals are modulated with the 4-Quadrature Amplitude Modulation (4-QAM). Also, we have eliminated the oversampling gain acquired during the baseband to IF conversion. This is given by $10 \log_{10}(f_s/f_{sys})$, where f_s is sampling rate and f_{sys} chip rate/symbol rate of DSSS/NB signal.

In Fig. 2(a) and 2(d), the BER of the DSSS signal and the NB signal with bandwidth of 1 GHz and symbol rate of 0.5 Gsps is shown, respectively, for different SF/symbol rates and as function of the signal to noise ratio (SNR). The BER of the DSSS signal decreases with an increase in SF (i.e., decrease in the symbol rate), which accounts for the increase in coding gain given by $10 \log SF$. There is a slight decrease in the BER of NB signal with the increase of SF of DSSS. This is due to the change in the PSD of the DSSS signal with the SF, which acts as an interference to the NB signal and depicted in Fig. 1. To understand the impact of the IF carrier frequency positioning within the DSSS bandwidth, we plot the BER for NB modulated over different IF frequencies in Fig. 2(b) and 2(e). In both cases, there is a small change in the BER. This further demonstrated the robustness of the system against a NBI anywhere within the bandwidth of interest. In Fig. 2(c) and 2(f), the bandwidth (symbol rate) of the NB signal is varied to observe the performance of DSSS and NB signals, respectively. The BER of the NB signal should remain the

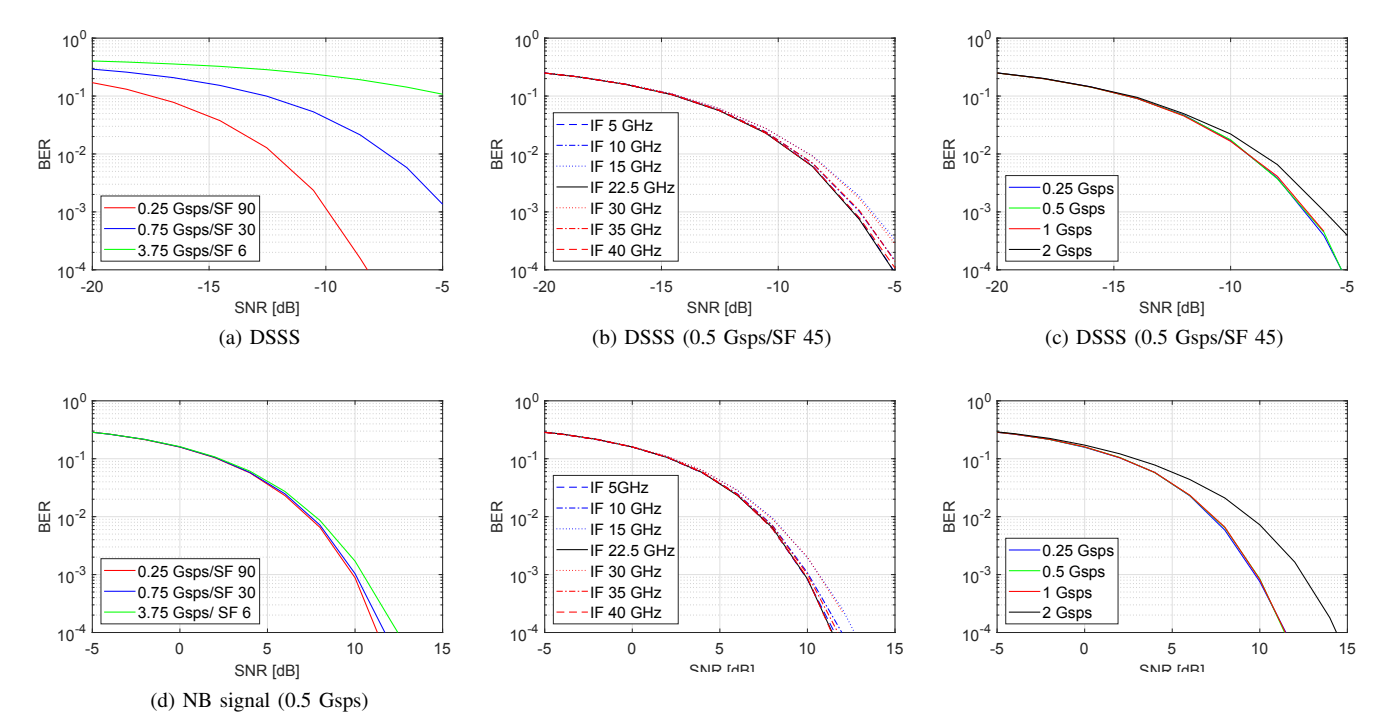


Fig. 2. BER for the 4-QAM DSSS (top) and various SF/symbol rate DSSS and fixed syn symbol rate of the NB signal.

same for all the symbol rates as we gain. However, the BER of the increment in bandwidth/symbol ra interference by the DSSS signal. A for the BER of the DSSS signal as

V. EXPERIMENTAL PERFORM

In this section, first, we discuss (hardware and software) to test the DSSS and NB systems. Then, the c in terms of BER with signal-to-i (SINR) are shown to demonstrate the presence of the other as interfe

A. Experimental Setup

1) Hardware: To evaluate the j and the NB signal, we simultaneous and a 1 GHz NB signal on the Tera system as shown in Fig. 3 [13].

At transmitter, the signals are loaded onto a state-of-theart Arbitrary Waveform Generator (AWG). This device can generate signals up to two channels, each having analog bandwidth up to 32 GHz, sampling rate up to 93.4 GSas. The IF signals (i.e., broadband DSSS and NB signal) are generated simultaneously from two separate channels of the AWG. To up-convert the signal to 130 GHz, two separate frequency multipliers (x4) and a mixer chain are utilized. A local oscillator (LO) signal is generated from an analog signal



Fig. 3. The experimental set-up consisting the AWG, two transmitters (one transmitting a DSSS signal and the other a NB signal), one receiver, and the DSO.

generator at 32.5 GHz and split by a divider to feed the two upconverters. The signals are transmitted through conical horn antennas with 10° half-power beamwidth and 21 dBi gain [13].

On the receiver, the two signals are received by a single down-converter chain. The receiver has a rectangular horn antenna with 25 dBi gain and 9° half-power beamwidth. The LO for the mixer is driven from a second signal generator of the same type. The received IF signal is captured by the state-of-the-art Digital Storage Oscilloscope (DSO), which has a high-speed ADC with a 160 GSas sampling rate for up to

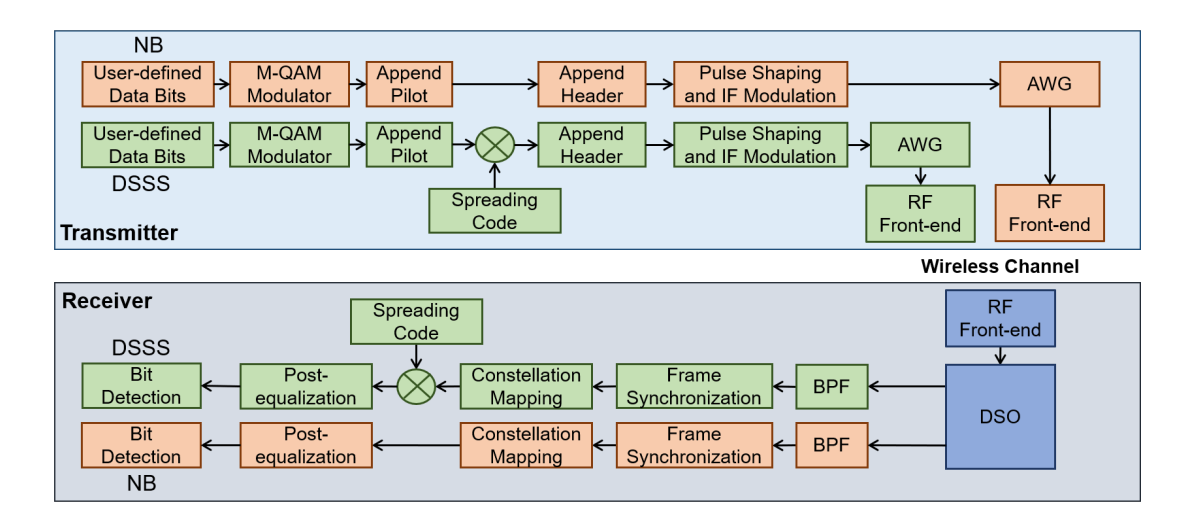


Fig. 4. Block diagram of the software based signal processing back-end for coexisting DSSS and NB users.

63.2 GHz of bandwidth [13]. The DSO digitizes, visualizes, and stores the received signal for further processing.

2) Software: The key digital signal processing blocks are shown in Fig. 4. At the transmitter, the user-defined data bits are mapped to the complex symbols (i.e., I + iQ) by an M-QAM modulator. The spreading code is utilized to spread the DSSS symbols into chips to occupy the available bandwidth. The symbols are encapsulated in frames by adding pilot (by using the same modulation scheme as data bits) and header (modulated using BPSK). The m-sequence of length 31 and length 127 (as modulating at chip rate) is used for the NB and the DSSS (without spreading the header) signal, respectively. Further, the NB symbols and the DSSS chips are pulse-shaped (by using Root-Raised cosine filter) and modulated at the desired IF band according to their corresponding symbol rate and chip rate, sequentially. The generated digitized samples of baseband/IF signal are fed to AWG for further up-conversion and transmission.

At the receiver, a band-pass filter (BPF) is used on captured IF signal to eliminate any out-of-band noise and interference. This step is crucial for eliminating DSSS interference and detecting the symbols of the NB signal. Thereafter, A similar header is utilized to detect the frame starting and synchronization. For further processing, the complex, i.e., I+jQ, received constellation points are recovered by low pass filtering by considering symbol duration and chip duration of NB and DSSS signal, respectively. For DSSS, the complex chips are despread to complex symbols by utilizing the same transmitter spreading code. A post-equalization filter is utilized to eliminate any frequency-dependent channel effect. Further, the symbols are mapped to bits by an M-QAM correlator type detector based on the maximum likelihood (ML) criterion.

B. Results

With the setup described, we transmit a series of broadband DSSS with 15 GHz of bandwidth and 1 GHz NB signals through the two transmitters, DSSS out of one and the NB

out of the other. Both the DSSS and NB signal have an IF center frequency of 7.5 GHz. For the DSSS signal, we consider 0.25 Gsps, 0.5 Gsps, and 1.25 Gsps signals with 4-QAM base modulation spread over 15 GHz bandwidth with SF 30, 15, and 6, respectively. Moreover, three types of 1 GHz NB modulated signals are considered: binary phase-shift keying (BPSK), 4-QAM, and 16-QAM; each signal has a 0.5 Gsps symbol rate.

To observe the effect of interference on each other, we transmit each of the DSSS signals along with each NB signal under different transmit power and link distance conditions. At distances of 1.5 m, 3 m, and 4.5 m, we capture 1) the NB and DSSS sent at the same power of 13 dBm 2) the NB signal sent at higher power (13 dBm) than the DSSS signal (3 dBm), and 3) the DSSS signal sent at higher power (13 dB) than the NB signal (3 dB).

Through offline processing, the BER for different SINR are evaluated to understand the performance of both the DSSS signals and the NB signal in the presence of one another. The grey coding scheme is considered for the base modulation schemes to obtain the BER. The post-processing SINR is considered to observe the effect on each other while demodulating the information-bearing baseband signal/symbol. The SINR is calculated by the error vector magnitude (EVM) of the received signal. The EVM of received/processed signal is measured by,

$$EVM = \sqrt{\frac{\frac{1}{N} \sum_{n=1}^{N} |S_{ideal,n} - S_{measured,n}|^2}{\frac{1}{N} \sum_{n=1}^{N} |S_{ideal,n}|^2}},$$
 (5)

where $S_{\mathrm{ideal},n}$ and $S_{\mathrm{measured},n}$ denotes the ideal constellation point transmitted and measured constellation point of the received signal after processing for nth symbol. N is the total number of symbols considered for the EVM calculation. The average SINR of the signal is estimated by averaging over EVM calculation of ten frames and given by,

$$SINR_{avg} = \frac{1}{EVM_{avg}^{2}}.$$
 (6)

In terms of post-processing, the SINR of broadband DSSS signal includes the despreading and oversampling gain of the signal. For NB signals, SINR incorporates the utilization of the bandpass filter to eliminate the out-of-band interference and noise. Moreover, ten frames are considered for BER estimation. In the point of fact, to have interference from each other all-time within the frame duration, various numbers of bits for DSSS and NB signal are considered. For DSSS (with 4-OAM), the minimum 1200 bits (for 0.25 Gsps signal with SF = 30) are considered, whereas the maximum goes to 3000 bits (for 1.25 Gsps signal with SF = 6). Similarly, for the NB (0.5 Gsps symbol rate/1 GHz bandwitdh) system, the minimum number of bits is 1200 (BPSK), and the maximum is 2400 bits (16-QAM). Also, the frames are transmitted in a synchronized manner. To demonstrate the BER performance on logarithmic scale, 0 BER is fixed to 10^{-6} .

It is observable by Fig. 5a the BER of DSSS scheme increases with the increase of symbol rate (i.e., with the decrease of SF and indicated by different symbol types) and distance (indicated by different color shades). Further, the BER increases for a higher level of interference, which is conceived by the different levels of transmit power for DSSS and NB systems. Similarly, in Fig. 5b, the BER of M-QAM rises with modulation order, distance, and interference level. Further, it is observable by Fig. 5c, the BER for 16-QAM decreases with an increment in DSSS SF (i.e., with the reduction of DSSS symbol rate). The reason behind the result is that with the increase in SF, the signal power gets spread over the bandwidth more uniformly, and hence the NB signal experiences comparatively lower interference (placed at the center IF frequency).

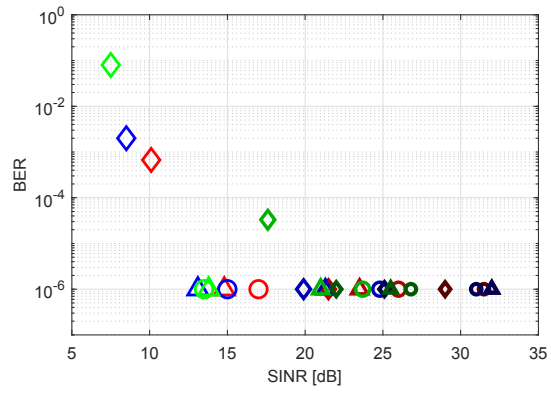
VI. STUDY CASE: COEXISTENCE BETWEEN ON THE GROUND ACTIVE USERS AND EARTH EXPLORATION SATELLITE SERVICES

To evaluate the interference to the passive sensing satellites, we consider the scenario in Fig. 6: a terrestrial link between two ground stations using directional antennas that could be interfering with a passive satellite orbiting at certain altitude.

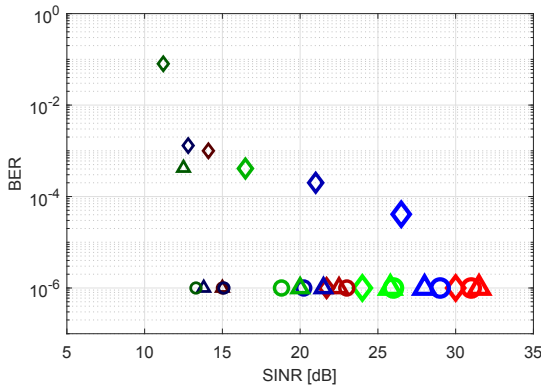
Considering the worst-case scenario when the satellite is pointing directly towards the ground transmitter, and assuming the total power is uniformly distributed over a spread bandwidth B, the interference power reaching the satellite is given by (in dB)

$$P_{\text{sat}}(f_c, h, \theta, d) = P_{\text{tx}}(f_c, d) + G_{\text{tx}}(\theta) - L(f_c, h, \theta) + G_{\text{sat}}^{\text{max}} + 10 \log \frac{B_{\text{ref}}}{B},$$
(7)

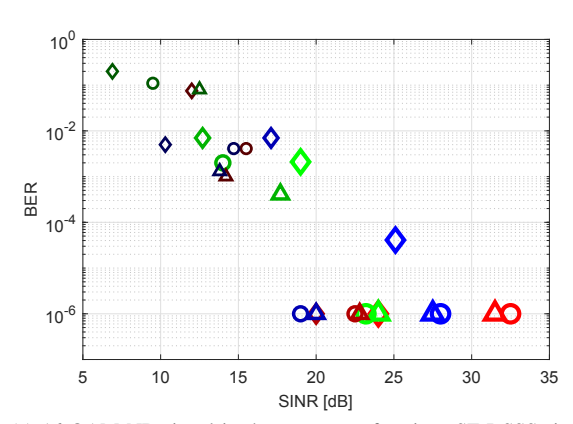
where $P_{\rm tx}$ and B are the transmit power and spread bandwidth respectively, necessary to create a terrestrial link at a distance d with a given data rate and error rate; L is the path loss for an Earth-space slant path with an elevation angle θ between



(a) DSSS signal in the presence of the NB signal (0.5 Gsps).



(b) M-QAM NB signal in the presence of 0.5 Gsps DSSS signal.



(c) 16-QAM NB signal in the presence of various SF DSSS signal.

Fig. 5. BER of DSSS and NB in presence of each other as interference. \bigcirc , \triangle , and \lozenge represents the 0.25 (SF = 30), 0.5 (SF = 15) and 1.25 (SF = 6) Gsps signals, respectively, for a) and c) and represents the BPSK, 4-QAM, and 16-QAM signals, respectively, for b). The color red, blue, and green symbolizes 1.5 m, 3 m, and 4.5 m, sequentially. Further, 1. DSSS and NB signal with 13 dBm and 3 dBm of transmit power, respectively, are shown by the darkest shade and smallest symbol size, 2. DSSS and NB signal with 13 dBm transmit power each are shown by the medium shade and medium symbol size, and 3. DSSS and NB signal with 13 dBm and 3 dBm of transmit power, respectively, are shown by the lightest shade and biggest symbol size.

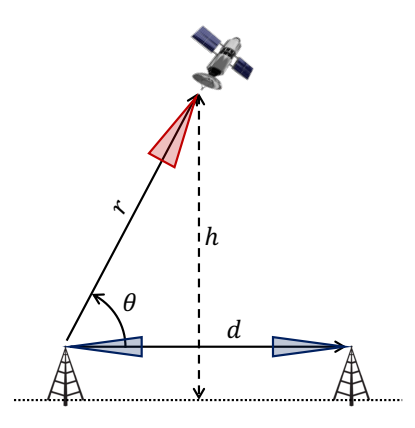


Fig. 6. Interference scenario between two ground stations separated at certain distance d and a satellite at a given altitude h and elevation angle θ .

the transmitter and the satellite, G_{tx} and G_{sat} are the antenna gains, and B_{ref} is the reference bandwidth of the satellite [4].

The Earth-space path loss L is modeled using the ITU-R models [14]–[18], which includes the conventional free-space path loss or spreading losses and the molecular absorption losses. The free-space path loss is due to the expansion of the wave as it propagates through the space, and the molecular absorption losses are due to the interaction of the electromagnetic waves with the air molecules of the atmosphere, mostly by water vapor and oxygen, which vibrate at specific resonant frequencies. The antenna radiation pattern also follows an ITU-R model [19], which models the gain as a function of the off-axis angle θ , and the maximum gain $G_{\rm max}$.

Fig. 7 shows the Earth-space slant path loss from a ground station to the Aura satellite at h=705 km for two frequencies at RR5.340 protected bands [20] that Aura's MLS utilize: 118 GHz and 190 GHz. The attenuation is minimum for a vertical path ($\theta=90^{\circ}$), i.e. the shortest path, and it increases with lower elevation angle. However, since the ground stations are pointing horizontally ($G_{\rm tx}^{\rm max}=G_{\rm tx}(\theta=0^{\circ})$), the gain also increases with lower elevation angles as depicted in Fig. 7.

The total transmit power necessary to create a 10 Gbps terrestrial link between two ground stations using 40 dBi antennas with a noise density $N_0 = 10^{-16}$ W/Hz [21], a low symbol error rate (10^{-5}) and different modulation orders is depicted as a function of the distance d in Fig. 8.

Finally, considering a reference bandwidth of 200 MHz and a satellite antenna gain of 40 dBi, the received power interfering the Aura satellite as a function of the elevation angle and the spread bandwidth is shown in Fig. 9. The maroon region represents the combination of elevation angles and spread bandwidth where the interference power is above the maximum interference level of -166 dBW for 118 GHz, and -163 dBW for 190 GHz, according to ITU-R Rec. RS.2017 [4]. The maximum interference happens for an elevation angle around 70° due to the trade-off between path loss and a lower antenna gain as illustrated in Fig. 9.

The results show that, for 1 km THz terrestrial link, with 5 GHz of bandwidth we are below the threshold at 118 GHz

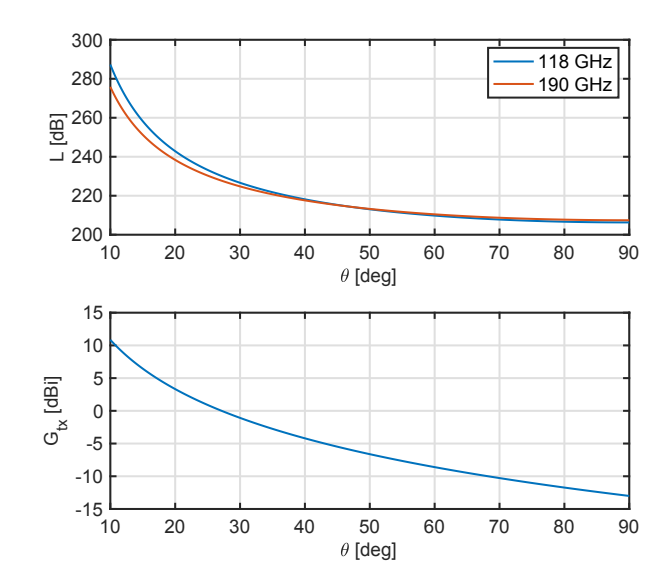


Fig. 7. (Top) Earth-space slant path loss from a ground station to Aura satellite for 118 GHz and 190 GHz as a function of the elevation angle θ . (Bottom) Directional antenna gain ($G_{\rm tx}^{\rm max}=40~{\rm dBi}$) as a function of the elevation angle θ .

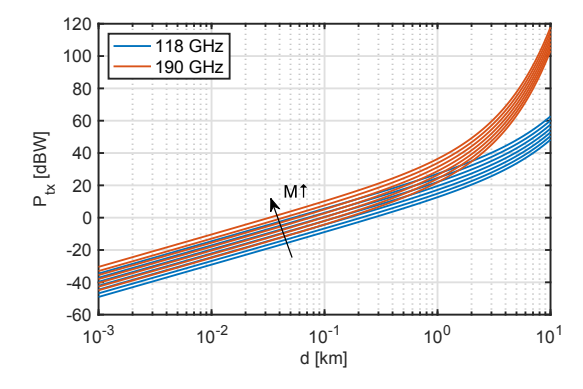


Fig. 8. Required transmit power for a terrestrial link as a function of distance for different modulation orders ($16 \le M \le 1024$) at 118 GHz and 190 GHz.

(Fig. 9a), whereas at 190 GHz, we need a spread bandwidth of at least 7.1 GHz (Fig. 9b). However for 3 km, we need a spread bandwidth of 12.2 GHz to be below the threshold for all elevation angles at 118 GHz (Fig. 9c), but at 190 GHz (Fig. 9d), the threshold is exceeded for angles above 30° even with 20 GHz of bandwidth since the necessary transmit power is much higher (Fig. 8).

VII. CONCLUSIONS

The DSSS system designed and tested in this paper demonstrates the technical feasibility of ultra-broadband spreading of signals for coexistence between passive and active users above 100 GHz. Traditional applications of DSSS techniques have only been used at slower data rates in applications such as GPS and CDMA communications. However, the advantages of spread spectrum modulation can be extended to high-speed communication by utilizing the very large bandwidth available above 100 GHz, which supports ultra-broadband spreading of

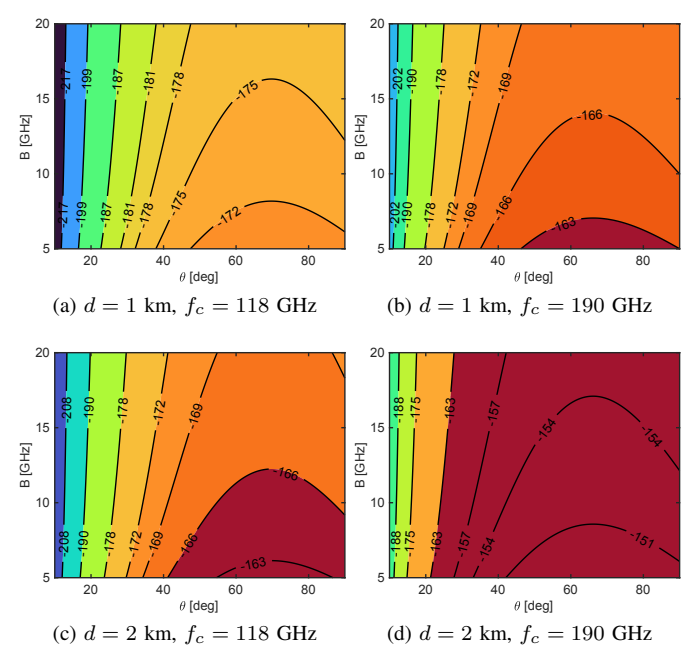


Fig. 9. Interference power in dB as a function of elevation angle and spread bandwidth at 118 GHz (Left) and 190 GHz (Right), and a required transmit power for a 1 km (Top) and 2 km (Bottom) terrestrial link. The maroon region represents the region where the threshold is exceeded.

signals while maintaining a high data rate for each individual user. In particular, using the state-of-the-art TeraNova testbed, we have demonstrated spread-spectrum signals with 15 GHz of bandwidth at 130 GHz. We have also showed the effectiveness of ultra-broadband DSSS in rejecting NB interference as well as coexistence with other passive users. This work serves as a proof of concept. Additional studies to explore the trade-offs between single- and multi-user data-rates, interference and coexistence, and security are part of the future work.

ACKNOWLEDGEMENTS

Northeastern University acknowledges the U.S. Government's support in the publication of this paper. This material is based upon work funded by AFRL, under AFRL Grant No. FA8750-20-1-0200. Any opinions, findings, and conclusions or recommendations expressed in this material are those of the author(s) and do not necessarily reflect the views of AFRL. Approved for Public Release; Distribution Unlimited: AFRL-2021-4246. This work was also partially funded by the US National Science Foundation (NSF) under grant CNS-2011411.

REFERENCES

[1] I. F. Akyildiz, J. M. Jornet, and C. Han, "Terahertz band: Next frontier for wireless communications," *Physical Communication*, vol. 12, 2014.

- [2] T. Rappaport, O. K. Y. Xing, S. Ju, A. Madanayake, S. Mandal, A. Alkhateeb, and G. Trichopoulos, "Wireless communications and applications above 100 ghz: Opportunities and challenges for 6g and beyond," *IEEE Access*, 2019.
- beyond," *IEEE Access*, 2019.

 J. W. Waters, L. Froidevaux, R. Harwood, R. F. Jarnot, W. R. H. M. Pickett, P. H. Siegel, R. E. Cofield, M. J. Filipiak, D. A. Flower, J. R. Holden, G. K. Lau, N. J. Livesey, G. L. Manney, H. C. Pumphrey, M. L. Santee, D. L. Wu, D. T. Cuddy, R. R. Lay, M. S. Loo, V. S. Perun, M. J. Schwartz, P. C. Stek, R. P. Thurstans, M. A. Boyles, K. M. Chandra, M. C. Chavez, G.-S. Chen, B. V. Chudasama, R. Dodge, R. A. Fuller, M. A. Girard, J. H. Jiang, Y. Jiang, B. W. Knosp, R. C. LaBelle, J. C. Lam, K. A. Lee, D. Miller, J. E. Oswald, N. C. Patel, D. M. Pukala, O. Quintero, D. M. Scaff, W. V. Snyder, M. C. Tope, P. A. Wagner, and M. J. Walch, "The earth observing system microwave limb sounder (eos mls) on the aura satellite," *IEEE Trans. Remote Sens.*, 2006.
- [4] ITU-R, "Performance and interference criteria for satellite passive remote sensing." Recommendation RS.2017, 2012.
- [5] M. Polese, X. Cantos-Roman, A. Singh, M. J. Marcus, T. J. Maccarone, T. Melodis, and J. M. Jornet, "Coexistence and spectrum sharing above 100 ghz," *Arxiv*, 2021.
- [6] W. Gao, Y. Chen, C. Han, and Z. Chen, "Distance-adaptive absorption peak modulation (da-apm) for terahertz covert communications," *IEEE Transactions on Wireless Communications*, vol. 20, no. 3, pp. 2064–2077, 2020.
- [7] J. Ma, R. Shrestha, J. Adelberg, C.-Y. Yeh, Z. Hossain, E. Knightly, J. M. Jornet, and D. M. Mittleman, "Security and eavesdropping in terahertz wireless links," *Nature*, vol. 107, 2018.
- [8] A.-A. A. Boulogeorgos, J. M. Jornet, and A. Alexiou, "A quantitative look at directional terahertz communication systems for 6g: Fact check," *IEEE Vehicular Technology Magazine*, 2021.
- [9] A. Hamza, A. Nagulu, A. F. Davidson, J. Tao, C. Hill, H. AlShammary, H. Krishnaswamy, and J. Buckwalter, "A code-domain, in-band, fullduplex wireless communication link with greater than 100-db rejection," *IEEE Transactions on Microwave Theory and Techniques*, vol. 69, no. 1, pp. 955–968, 2020.
- [10] B.P.Lathi, Modern Digital and Analog Communications Systems. Oxford University Press, 3rd ed., 1998.
- [11] A. Goldsmith, Wireless Communications. Cambridge University Press, 1st ed., 2005.
- [12] B. Sklar, Digital Communications. Prentice Hall, 2nd ed., 2001.
- [13] P. Sen, D. Pados, S. Batalama, E. Einarsson, J. P. Bird, and J. M. Jornet, "The teranova platform: An integrated testbed for ultra-broadband wireless communications at true terahertz frequencies," *Elsevier Computer Networks (COMNET)*, vol. 179, October 2020.
- [14] ITU-R, "Calculation of free-space attenuation." Recommendation P.525, 2019
- [15] ITU-R, "Attenuation by atmospheric gases and related effects." Recommendation P.676, 2019.
- [16] ITU-R, "Reference Standard Atmospheres." Recommendation P.835, 2017.
- [17] ITU-R, "The radio refractive index: its formula and refractivity data." Recommendation P.453, 2019.
- [18] ITU-R, "Analytical method to calculate short-term visibility and interference statistics for non-geostationary satellite orbit satellites as seen from a point on the Earth's surface." Recommendation S.1257, 2002.
- [19] ITU-R, "Reference radiation patterns for fixed wireless system antennas for use in coordination studies and interference assessment in the frequency range from 100 MHz to 86 GHz." Recommendation F.699-8, 2018.
- [20] ITU, "Radio regulations," 2020.
- [21] P. Sen, V. Ariyarathna, A. Madanayake, and J. M. Jornet, "A versatile experimental testbed for ultrabroadband communication networks above 100 ghz," *Computer Networks*, vol. 193, p. 108092, 2021.